

Original Article

Assessment of a Linear Phased Array Transducer Parameters for Brain Stimulation

M. Salehnia^{1,2}, H. Ghadiri^{1,2,*}

1- Department of Medical Physics and Biomedical Engineering, Tehran University of Medical Sciences, Tehran, Iran.

2- Research Center for Molecular and Cellular Imaging (RCMCI), Tehran University of Medical Sciences, Tehran, Iran.

Received: 4 March 2017

Accepted: 25 May 2017

Keywords:

Transcranial Focused Ultrasound,
Phased Array Transducer,
Brain Stimulation,
Neural Network.

ABSTRACT

Purpose- Transcranial Focused Ultrasound (tFUS) is a safe method with high resolution to stimulate the brain tissue. By appropriate beam-forming, using a phased array transducer enables us to focus on the desired position with high resolution without moving the transducer.

Methods- In this paper, the physics of tFUS propagated from a linear phased array transducer, in a 2-dimensional environment, is simulated using the k-space pseudospectral method. Furthermore, we study some factors affecting the spatial accuracy of focus point including the length of the transducer and its elements, the beam-forming and the amplitude of input pressure signal. Also, the thickness of the bone layer and the depth of focus as environmental features are considered subsequently.

Results- We investigated these parameters to propose optimum conditions in the transcranial focusing. The main contribution of this research includes: 1. Computing tissue-sensitive time delays of transducer elements, 2. Providing a minimum possible length of the transducer and 3. Using a neural network to determine the best possible value of the amplitude of the input pressure to get a desired focus pressure that was not possible before.

Conclusion- Based on our experiments, we obtain a significant decrease of about 32 units in the maximum error and fit a function to estimate the pressure with a correlation coefficient of approximately 0.9997.

1. Introduction

Brain stimulation is a process of stimulating the activity of specific areas in the brain, like the visual cortex or the motor cortex. Brain stimulation causes an increase or decrease in amplitude of evoked potentials [1]. The brain mapping can be achieved by identifying the nodes in brain networks, that their modulation causes changes in mental experience and behavior [2]. So, the stimulation of the brain tissue can be used

for brain mapping. Also, the therapeutic utility of noninvasive brain stimulation has been claimed for various neurological and psychiatric disorders such as depression, schizophrenia, Parkinson's disease, dystonia, epilepsy and so on [3]. Therefore, brain stimulation is an essential and practical subject in medical sciences.

Conventional approaches to stimulate the brain circuits face some limitations. Electrical deep brain stimulation presents precise targeting; however, it

***Corresponding Author:**

Hossein Ghadiri, PhD

Department of Medical Physics and Biomedical Engineering, Tehran University of Medical Sciences, Tehran, Iran.

Tel: (+98)2166439831 / Fax: (+98)2166438630.

Email: h-ghadiri@tums.ac.ir

needs invasive procedures to plant the electrodes [4]. Although, the optogenetics, which uses light to activate the ion channels, has an excellent spatial resolution as it uses genetics changes, it may pronounce some level of invasive procedures [5]. Both Transcranial Magnetic Stimulation (TMS) and transcranial Direct Current Stimulation (tDCS) are non-invasive techniques; however, they suffer from low spatial resolutions [6], and some level of harmfulness [7]. In comparison with methods mentioned earlier, the transcranial Focused Ultrasound (tFUS) is a developing method with some known advantages such as: completely non-invasive functionalities, relatively high spatial resolution, and focusing in deep brain structures. However, we should be aware of the potential of the biohazardous effect of ultrasound (thermal fluctuations and/or cavitation damage) by considering the energy deposition of ultrasound to tissues [8].

Focused ultrasound has been used for neuro-modulation purposes. Tufail *et al.* investigated the effect of transcranial pulsed ultrasound on the motor cortex of mouse brain [9]. They approved that the ultrasonic stimulation of neuron activity causes evoking motor behaviors. Yoo *et al.* stimulated the somatosensory and visual regions of a rabbit's brain by a spherical ultrasound transducer [10]. They found out that the modulatory effects of Focused Ultrasound (FUS) can stimulate or suppress the brain activity. They reported that no tissue damages happen after applying FUS. Mulgaonkar *et al.* attempted to manipulate a prototype of a low intensity focused ultrasound stimulator system to stimulate the brain of Göttingen minipig, as a large animal model [11]. They stimulated the hypothalamus of the minipig that led to temporally correlated increases in both heart rate and blood pressure. Lee *et al.* applied the tFUS on s1 region of somatosensory cortex of human samples [12]. They found that a low intensity focused ultrasound can naturally elicit the tactile sensations and also lead to a cortical evoked potential in human samples. After that, Legon *et al.* followed the experiments on human samples, and examined the effect of tFUS on s1 region of the human brain. They found that tFUS can modulate the cortical function of human brain locally [13]. Mueller *et al.* constructed a computational model of transcranially focused ultra-

sound based on acoustic tests in a water tank [14]. Then, they extended the model to investigate the effects of tissue properties and geometry on the wave propagation. Finally, they modeled the heating caused by ultrasonic stimulation waveforms which is produced in tissues. They showed that the brain anatomy and biological material properties have some effect on propagating of ultrasound waves and result in safe heating levels in the skull and brain. Nowadays, the development of experimental and clinical tFUS systems [15] and its effect on different regions of the brain [16] are known as exciting discussions in this field.

The Phased Array Transducers (PATr) are able to effectively focus and steer the ultrasound waves for tFUS applications [12, 13]. Actually, the waves generated by a PATr are focused or steered by the time delays of each signal element [17]. Using PATr, we do not need to move the transducer in order to change the position of target. An appropriate beam-forming can be applied to change the position of the focal region, where the point of interest inside the brain should be precisely stimulated. However, as the skull has different acoustic properties, this procedure for brain targeting will be impaired [18]. PATr systems have been developed for brain surgery and the disruption of blood brain barrier. For instance, Hynynen *et al.* offered a 500-element PATr all with the same size [19]. It was operated at a frequency of 700-800 kHz and was used for thermal ablation successfully. Liu *et al.* designed a prototype of a focused ultrasound system for non-invasively blood-brain barrier disruption [20]. This system was a hemispherical, multi-channel phased array operated at a frequency of 200-400 kHz. Their results showed that this fabricated PATr system is capable to focus on both centered and off-centered geometries, with an acceptable power and ready to be developed for clinical applications.

According to the different applications and importance of focused ultrasound for stimulation of brain tissue, it is essential to design and fabricate an optimum ultrasound transducer. As far as we know, most of researches in this context use instruments in which a single-element transducer is utilized for ultrasonic wave generation. However, based on obvious advantages of PATr in comparison with the single-element transducer, some researches have been done to propose this type of ultrasonic transducer, i.e. Law Wing *et al.*

introduced ultrasound phased array apparatuses and methods for making and using them. Their patent included some methods to manufacture thin and lightweight apparatuses [21]. For example, they offered to use a Surface Mount Technology (SMT) or similar approaches to manufacture small, lightweight, and energy efficient ultrasound arrays. Alternatively, they suggested arranging an array of ultrasound transducer elements on a Printed Circuit Board (PCB). The PCB may be rigid or flexible. Therefore, the design of the transducer can be changed according to its application. These characteristics (including being thin, lightweight and flexible) allow the array to be worn on a subject's head or other body regions. So, these arrays are introduced as an excellent gadget for neurostimulation. The state of the art and advanced methods to manufacture the ultrasound phased array, help us design an apparatus for each application. Unlike traditional phased arrays, as these methods are not expensive, we can design our desired array according to our needs.

Based on apparent advantages of PATr in comparison with the single-element transducer, the current article studied the PATr used in tFUS. In this paper, our goal is to investigate how the different parameters of PATr can affect the tFUS procedure. We tend to investigate the factors influencing the position, pressure, and size of the Focal Point (FP) when a tFUS system is used. These factors include the transducer and elements size, the amplitude that is generated by the elements, beam-forming method, and the effect of bone layer thickness (according to the position of the transducer). Studying these factors help us design an appropriate transducer. For example, to stimulate a specific area of the brain with a desired intensity and resolution, it requires extracting the transducer's features. These features help us manufacture the particular phased array according to the desired stimulation condition. As the new technologies make the manufacturing of the phased arrays easier and cheaper [21], by considering these parameters, we can produce them purposefully.

We investigated the relation between PATr parameters and the parameters related to the brain stimulation. To achieve this aim, we considered a linear PATr appropriate for brain stimulation. Then we attempted to examine the different values of PATr's parameters and investigated their effects on the stimulation condition. Optimizing factors mentioned above related to the PATr, lead us to present some data for designing a PATr of a different condition for brain stimulation. More precisely, according to the desired condition of stimulation, we will be able to define the physical properties of PATr and its beam-forming.

2. Material and Method

2.1. Simulation Method

K-Wave is an acoustics toolbox for MATLAB that presents an advanced time-domain model of acoustic wave propagation¹. This toolbox uses the k-space pseudospectral method to solve the acoustic equation. It reduces memory and time steps of simulation [22]. The physics of tFUS, which is produced by a PATr was simulated using this toolbox.

2.1.1. Geometry of Simulation

The geometry of simulation is shown in Figure 1, in which a 2-dimensional medium with acoustic properties of the brain is simulated. We defined a bone layer, adjacent to the transducer. So, the simulated medium consists of the brain and skull and both of them are considered as a homogenous tissue. The acoustic properties of mediums that were used are defined in Table 1. Calculations have been performed in a computational grid with a 0.46 mm grid point size. This value has been chosen according to the Nyquist limit of two grid points per wavelength [23]. An absorption layer has been defined around a computational grid with thickness of 0.92 cm, for absorbing the acoustic waves when they reach the edges of the computational domain.

¹ <http://www.k-wave.org>.

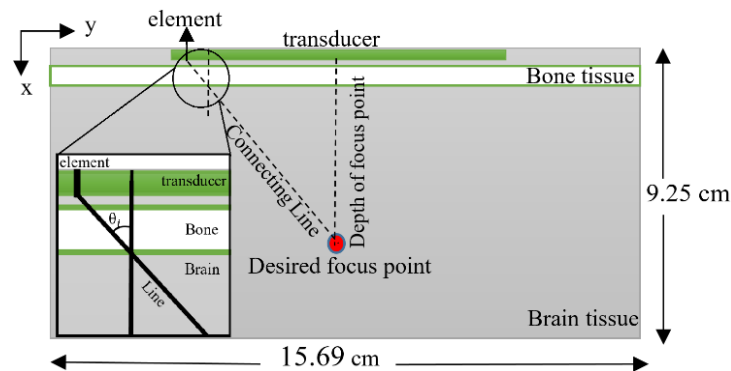


Figure 1. 2-dimensional simulated medium and the linear phased array transduce.

Table1. Acoustic properties of tissues in the head [24].

Tissue	Acoustic Absorption Coefficient (dB/(cm MHz))	Density (kg/m ³)	Sound Speed (m/s)
Brain	0.58	1040	1560
Bone	3.5	1990	3200

2.1.2 Simulation of Transducer

According to previous investigations, at frequencies of less than 0.5 MHz, it is possible to reach an appropriate power to stimulate the brain tissue [25]. Moreover, at this range of frequency, the malformation of ultrasound beam which is caused by the skull, is lower compared to the higher frequencies. The reason is, in the low frequencies, the skull thickness is thinner in comparison to the wavelength. Hence, we have chosen the frequency of 0.5 MHz for waves to be propagated in the medium. We have defined a linear PATr for our experiments.

2.1.3. Simulation of Focusing Procedure (Transducer's Beam-Forming)

After the implementation of the geometry and a linear PATr (according to Figure 1), the waves were focused on different positions. To focus the waves, we assigned a particular time delay for the wave propagated from each element of the transducer. These delay-times were calculated according to the distance of elements to the FP and the speed of sound in the medium. We used a pulsed pressure wave (single-cycle Tone Burst) in the simulation.

The waves were focused in two different situations: where there is not any bone layer, and in the latter one a bone layer, as the skull, was considered in the path of the ultrasound beam.

In the focal region, we defined the point with the maximum pressure as FP. The FP algorithm was designed to do this by searching the whole focal region in all simulation steps and return the FP as a unit point. The spatial distribution of pressure was obtained for the two situations. The pressure distribution helps us make sure of spatial and temporal focusing.

2.1.4. Validation of Simulation Method

Mueller *et al.* have investigated how tissue properties affect the wave propagation in the context of tFUS [14]. They have also studied the associated heating in the different layers of the head. They did some empirical research in a water tank and then carried out some computer simulations to investigate the different conditions of head geometry and its layers in neuromodulation procedure.

To validate our simulation method, we used the laboratory condition of a water tank in Muller's experiment. So, we focused the waves at the geometric centre of the hemispherical transducer with our simulation method (k-space pseudospectral method). We compared the Spatial peak-pulse average Intensity (I_{sp}) of our computational model and experimental data of water tank. This comparison helped us understand the accuracy of our simulation method.

2.2. Improvement of Beam-Forming Method (Optimized for Skull)

The FP position obtained by the FP algorithm was compared with desired FP coordination. We found out that the FP has been displaced by 1.4 *cm* in the presence of the bone layer. This displacement occurred because the bone layer acts as a heterogeneous factor in our simulated homogeneous environment. Therefore, it changes the sound speed in wave path and it influences focusing procedure. Furthermore, it is essential to consider the bone layer in the time-delay calculations.

To study the effect of using a bone layer in front of the transducer on the coordination of FP more precisely, a different thickness of bone layer has been defined, while the position of the desired FP was fixed. The range of the thickness of skull is measured in literature from 5.3 *mm* to 7.5 *mm* [26]. However, here we have increased the thickness to 1.38 *cm*. This helps us judge the trend of changing. Besides, the bone layer was just an index of the heterogeneity of environment. The FP coordination has been obtained using the FP algorithm. The difference between the coordination of this point compared to the point targeted as the FP has been calculated. The results are shown in Section 3.3. We investigated the reason of error in targeting and presented an algorithm to improve it. This algorithm considered all the mediums in the path of the wave to calculate the time delays. In other words, we used a new tissue-sensitive beam-forming method for our transducer. So, we considered the bone layer, by using an average of sound speed for each ray, which is traversing the medium in our computations (results are shown in Section 3.3). This algorithm is called the “improved focus function”.

2.3. The Effect of FP Depth

We studied how the depth of focus affects the accuracy of the position of the FP, after using the “improved focus function” algorithm. Actually, we investigated the efficiency of aforementioned algorithm in different depths. In order to focus in different depths, we changed the x-coordination of FP from 1.84 *cm* to 7.82 *cm* (the y-coordination is fixed). The transducer size was 5.98 *cm*. More precisely, 130 pressure sources with the same size

of a computational grid point have been defined as a linear PATr. The thickness of the bone layer was 0.69 *cm*, as the average thickness of the skull [26]. The simulation was performed using the “improved focus function” and compared with the original focus function. The results are shown in Section 3.2.

2.4. The Effect of Transducer/Element Size

At the next step, we investigated how the length of transducer affects the FP specification, including pressure and coordination. We considered the element length is equal to 0.046 *cm* and the geometry of simulation is the same as before. The thickness of the bone layer was defined as 0.69 *cm*. Here, different depths were selected as our targets; for example, 2.76 *cm*, 4.6 *cm*, and 6.44 *cm*. By choosing the depth of 6.44 *cm*, the ability of deep focusing using linear PATr is examined.

In each depth, different transducer lengths were used to focus and measure the pressure and coordination of the FP. Therefore, we can find out that for which length of the linear transducer, the least error and the most accuracy are obtained. The length of the transducer was increased by 17.9 *cm* with steps 0.046 *cm*. Note that the position of the transducer was fixed at the middle of the calculation grid. So, the increase of the transducer’s length was done by adding elements to the outer edges of the transducer. The results are shown in Section 3.5.

Also, we tended to investigate the effect of element size. As we mentioned, each pressure source has a dedicated time delays. Here, we defined more prominent elements by grouping several sources and assigning the same time delay to the group. Our goal was to investigate how the element length affects the position of the FP. According to our results in Section 3.5, the transducer length was chosen 5.56 *cm* as an optimum length. We defined the element as a group of sources which are activated at the same time with the same time delay as beam-forming. The element’s time delay was considered as a mean of time delays of sources making the element. We defined different sizes and focused on different depths. Then, we calculated the absolute error of the FP position for each desired depth. We showed that our results for six sizes and 14 depths which is explained in Section 3.5.

2.5. The Effect of the Depth, Bone Thickness and Element's Pressure on the Amplitude of Focus Pressure

We studied the effect of the depth, the thickness of the bone and the length of the transducer on the position of the FP. The bone thickness and depth caused a displacement of the FP and we reduced this displacement by performing an algorithm which is explained in Section 2.2. Also, we were able to find an optimum length of the transducer (according to results in Section 3.5). Additionally, we investigated that the amplitude of the elements pressure does not have any effect on the position of the FP.

In this Section, we studied the effect of the focus depth, bone thickness and amplitude of element's pressure (we call it as input pressure) on the pressure of the FP simultaneously. The goal was to present a method to indicate the element's amplitude of pressure for a given depth, bone thickness, and desired pressure of the focus.

We set up an experiment, which considered different conditions to estimate the correct relation between input and output pressure. To do this, the waves were focused in different situations, by considering eleven bone thicknesses, ten amplitudes, and seven depths; when the length of the transducer was set to 5.56 cm, as the optimum

length. The results are presented in Section 3.5. We recorded the pressure in the FP for all 770 cases. To have a comprehensive point of view, in which all affecting parameters are considered, we tried to obtain a function that can predict the relation of these parameters. As it was a multi-parameter problem, determining a function was not straightforward. For this purpose, we used Weka . The Machine Learning (ML) algorithms helped us get a function (model) that can map the input to the output. We tried four different ML algorithms to learn how our three parameters affect the amplitude of focus pressure. By considering that the depth and thickness were known as the input for our problem and cannot be changed by our method, hence, using ML algorithm [27], the input amplitude can be tuned to obtain the desired amplitude in the FP. In other words, we tended to determine the appropriate input amplitude of the elements pressure, according to the desired amplitude of pressure in the FP, the thickness of the bone layer, and the depth of focus. To evaluate these algorithms, a 10-fold cross validation was used [28]. Based on the result of Table 2, we have selected a Multi Layer Perceptron (MLP) which is known as a kind of Neural Network (NN) [29], as an appropriate tool in order to fit the function. The reason was that it gave a model with the highest correlation coefficient and the lowest error.

Table 2. Errors of training data for four different algorithm.

Algorithm	Correlation Coefficient (Higher is Better)	Mean Absolute Error % (Lower is Better)	Relative Absolute Error % (Lower is Better)
Regression By Discretization [30]	0.9703	0.0869	17.3667
Linear Regression	0.9700	0.0949	18.9507
MSP [31]	0.9918	0.0489	9.7717
MLP	0.9997	0.0103	2.0539

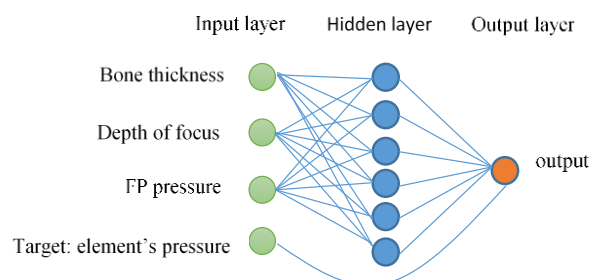


Figure 2. Neural network architecture for estimating the relationship of input parameters.

2.5.1. MLP Algorithm as a Modeling Tool

MLP is a kind of NN which is used to solve multivariable problems by nonlinear equations using a training process. It uses an error back propagation technique for training from the input data [32]. The architecture of an MLP consists of three layers known as an input layer, hidden layer, and an output layer. There are some neurons or units in each layer. These units receive their input from units in the last layer and applied their activation function to the sum of the weighted input. The output of the function is sent to neurons in the next layer. This process is repeated, and finally, output values are obtained in the output layer. At the end of each training iteration, the MLP's output is compared with the desired target (gold data) and the error is computed. Finally, the error is back propagated to previous layers to tune the weights. In our study, the input data of MLP were the thickness of the bone layer, the depth of focus and the recorded pressure of the FP. The

input amplitude was set as the target. Therefore, the weights were adjusted by calculating the error of the predicted target value and the actual target value (back propagation technique) in each epoch. The output of our MLP is a model which defines the relationship of input parameters. Also, the hidden layer consists of 6 neurons. Figure 2 illustrates the architecture more clearly. Figure 3, shows how the change of these values influences the accuracy of our model. In Figure 3a. the learning rate is fixed to 0.3 and in Figure 3b. the momentum is fixed to 0.2, however, for different learning rates and momentums the same behavior was seen for values less than 0.5. This means that we have an acceptable correlation coefficient in this range. So, the learning rate and momentum of our NN was set 0.3 and 0.2, respectively. The number of the epoch was fixed to 500, and we used a 6-neuron hidden layer MLP. By this model which is trained by MLP, we expected that the input pressure can be predicted for a desired pressure of the FP.

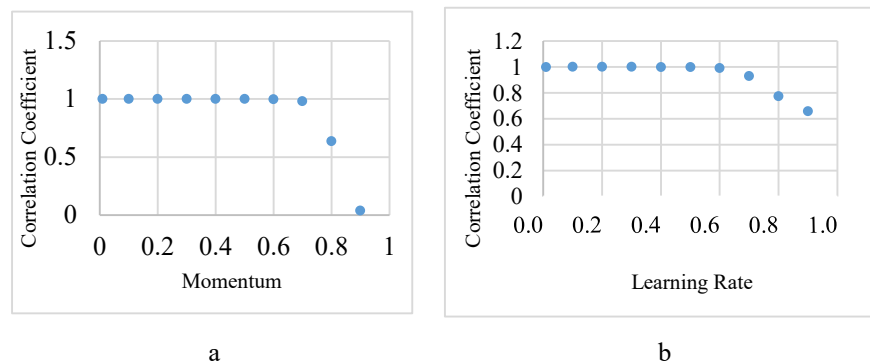


Figure 3. Correlation coefficient as the function of a) momentum (with learning rate of 0.3) and b) learning rate (momentum of 0.2).

As we explained before, the goal of using MLP was to estimate the relation between the thickness of the bone layer, the depth of focus, the amplitude of element's pressure, and the FP pressure. This relation can be presented as a model or function by MLP algorithm as a universal approximator [33]. We considered three parameters of thickness, depth and element's pressure as the input of simulation. The FP pressure obtained from simulation is related to the physics of focusing procedure in the environment. Therefore, the relation of these four parameters (inputs and output of simulation) explains the condition of the wave propagation which we do not have enough perception about it. Accordingly, our problem is known as an inverse model problem and we have tried to solve it using

MLP. Moreover, we can use it to estimate the amplitude of the element's pressure.

Finally, to show the efficiency of our model obtained from MLP, we used the model obtained from MLP, for 770 different conditions (10 different pressure of FP and 77 different depths and bone layer thickness) to estimate the pressure of the elements. Then, we used these pressures in the simulation; and we compared the output pressure in the FP (obtained after simulation) with the pressure of the FP which we used as the input of the model.

The steps of the method are summarized as a process flowchart (Figure 4).

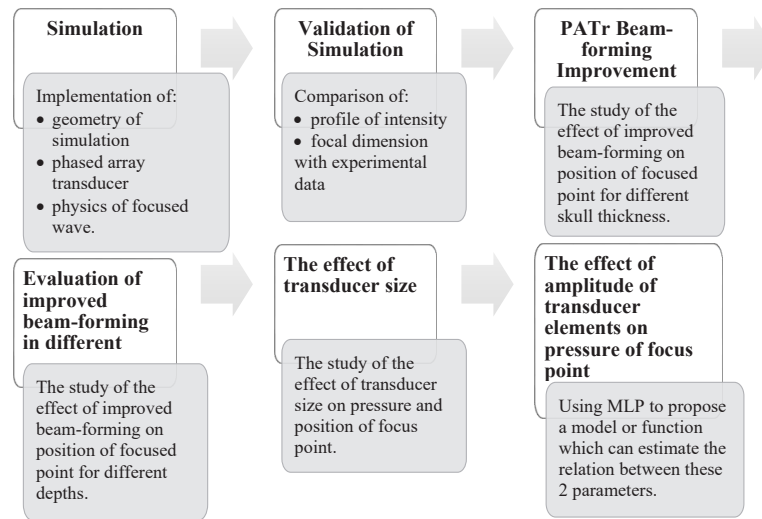


Figure 4. The process flowchart of method.

3. Results and Discussion

3.1. Simulation of Focusing Procedure (Transducer's Beam-Forming)

At the first step, we tried to simulate the physics of the focused ultrasound by our simulation tool. The pressure obtained in the FP is 2.4 MPa ($I_{sptp} = 241.6 \text{ W/cm}^2$). There is no displacement in the FP in the absence of bone layer; although by using a 6.9 mm bone layer, a 1.47 cm shift is seen. Note that no displacement in y-direction is seen. In this case, the pressure of the FP is 0.64 MPa ($I_{sptp} = 22.7 \text{ W/cm}^2$), showing a reduction in the pressure. Aforementioned results indicate that there exists an attenuation of waves in the bone layer.

Figure 5a illustrates the distribution of the acoustic pressure waves around the FP during the whole simulation time, without any bone layer. As the propagating waves from the transducer are formed as a pulse wave of one cycle, an outline of continuous wave field can be seen. The reason for choosing such a display is a better perception of how focusing occurs in both temporal and spatial dimensions. Figure 5 shows the result of focusing the ultrasound waves by our simulation method. In Figure 5, we can see a focus region for both cases (presence and absence of the bone layer) we considered. However, when we used a bone layer, this region is shifted to the bone layer. Also, there are high amplitudes of pressure in the bone layer (Figure 5b).

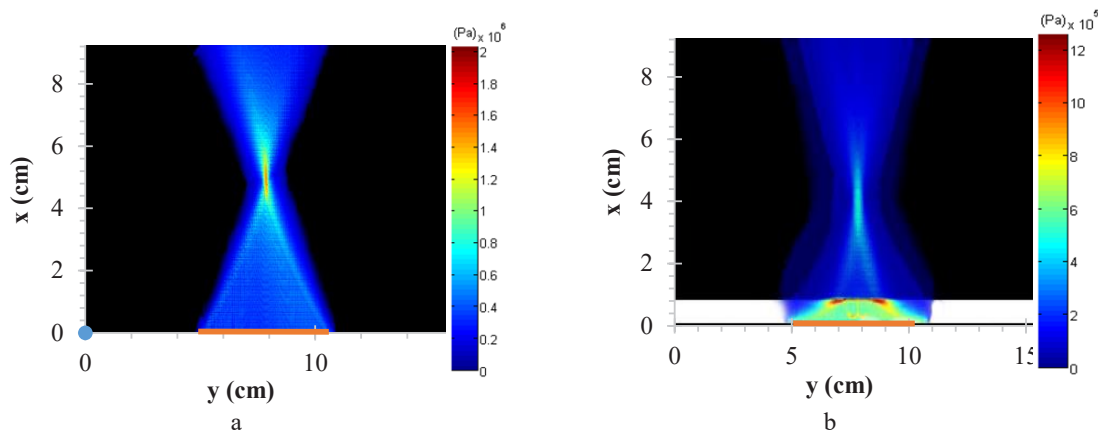


Figure 5. The pressure distribution aggregated during the whole simulation time in a 2-dimensional medium (a) absence (b) presence of the bone layer) where a pulsed wave is focused. The position of the transducer is shown with a red line. The amplitude of pressure wave of transducer is 0.8 MPa [34].

3.2. Validation of the Simulation Method

Mueller *et al.* focused the ultrasound waves by a single-element hemispherical transducer in the water tank. They put a layer of skull in front of the transducer. We simulated the same condition of their experiment and reported the Isppa. The hydrophone measurements gave an Ispps of 5.90 (W/cm²), and the results of our simulation showed an Isppa of 5.95 (W/cm²). So, a relative error of 0.84 is obtained. According to this result and some results obtained from the simulation of free water and transcranial model, we can introduce our simulation which is developed, as a reliable method for the focused ultrasound. Therefore, we used it for our investigations and the development of the linear PATr.

3.3. Improvement of Beam-Forming Method (Optimized for Skull)

We investigated the effect of heterogeneities of tissue on the accuracy of targeting by increasing the bone layer thickness. The diagram in Figure 6 shows that as the thickness of the bone layer is increased, the waves are focused earlier and closer to the bone. As indicated in Figure 6, when the thickness of the bone layer is 1.38 cm, the ultrasound wave is focused in the depth of 1.88 cm, instead of 3.68 cm (our desired). The maximum relative error in the displacement is 48.75 percent when 1.38 cm of the thickness is used (Figure 7a). These errors in the position of the focus point are related to an inaccurate focus function being used, in which time delays are not calculated precisely. The bone layer makes the waves to be propagated faster. The distance, which the waves

have to travel through the bone layer, is different depending on the position of source elements on the transducer. For example, the waves propagated by the elements that are placed at the tail of the transducer, travel more distance compared to those that are near the center. So, it is expected that the waves arrive in phases at a closer point if the bone layer is ignored in time delays calculations. Therefore, considering the different tissues in the way of the wave propagated from each element is important. The independence of this error to the density and attenuation coefficient of the medium has been previously investigated.

It is required to calculate the precise sound speed in the medium, for computing the appropriate time delays. In this paper, we proposed an algorithm to find the best time delays of the transducer elements (named the “improved focus function”). This algorithm is tissue-dependent, which means that different acoustic specifications of different tissues that ultrasound waves are propagated are considered in our computations. To be more precise, this algorithm considers the distance between each element and the desired FP and all the points in the connecting line in Figure 1 to compute the average sound speed. Hence, this algorithm offers an adaptive sound speed for each element and finally calculates the time delays. The error of the FP displacement has been brought to below 16.25% (Figure 7b), and this means an impressive improvement of 32.5 unit. Figure 8 shows the position of the FP in the x-direction for different thickness of the bone layer using an improved focus function. As you can see, there is a low shift in the position of the FP after applying the algorithm as a new focus function.

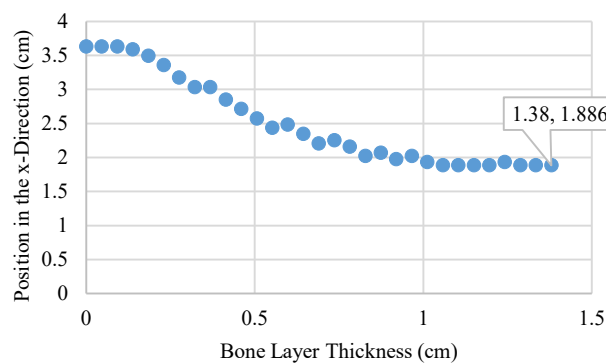


Figure 6. The relative error in x coordination of FP as a function of bone layer.

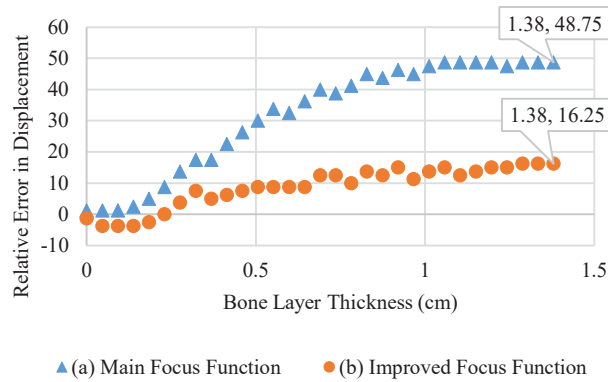


Figure 7. The x coordination of the FP as a function of the bone thickness.

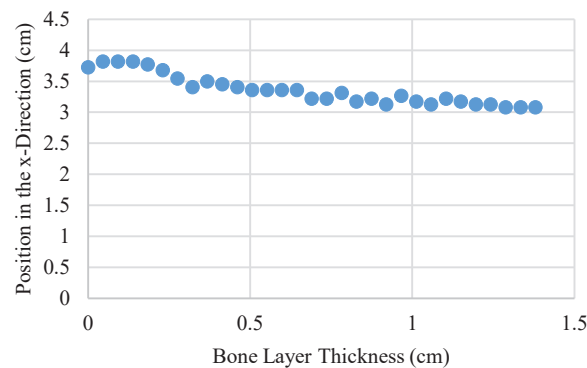


Figure 8. The x coordination of the FP as a function of the bone thickness after using the improved function.

3.4. The Effect of FP Depth

We changed the depth of the target and then we found the real point of focus for our FP algorithm (explained in Section 2.1.3). These experiments were done with a main focus function and an improved focus function.

As you can see in Figure 9, as the depth increases, the absolute error increases. We had shown the results for both conditions when we used

the primary focus function (Figure 9a) and the “improved focus function” (presented in Section 2.2) (Figure 9b). As you can see, our improved focus function causes to obtain less error in all depths.

Because we have used the average as our measure, the thin bone layer does not play a notable role for deeper points. So, it is worth trying to offer a new focus function to act more efficiently in the deeper tissues in order to decrease the focus displacement.

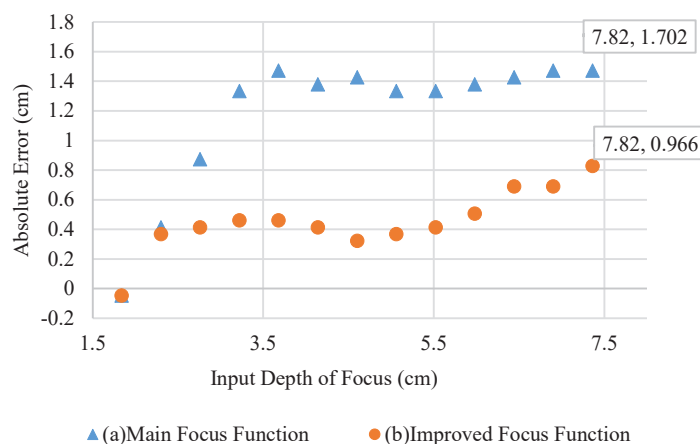


Figure 9. The absolute error of the focus depth for different depth of focus.

3.5. The Effect of Transducer/Element Size

In this Section, the effect of transducer length on the position of the desired FP and the pressure were investigated using a PATr. The length of the transducer was increased by 17.9 cm with steps of 0.046 cm. The position of the transducer was fixed in the middle of calculation grid. Increasing the transducer's length was done by adding elements, with the size of 0.046 cm, to the end sides of the transducer. The position of the focus point and its pressure were recorded for different lengths. We show these results for 3 depths as a sample in Figure 10 and Figure 11.

In each depth, after a threshold of transducer length, the waves are focused nearly on the target (Figure 10a). The aforementioned issue happens earlier in low depths. Figure 10b shows the relative error in the position of the focus point for different transducer lengths in each of the three depths. For different depths, we can choose the length of the transducer equals to a quantity that there is no change in targeting error for greater values (targeting error is defined as the difference between the desired focus position and actual focus position). According to these results, the transducer length of 5.56 cm is the smallest length in which the error is less than 15 percent. It means that if we choose this length, then we have a low error for different depths. However, increasing the length of this amount will not decrease the targeting error. So, it can be known as an appropriate length for linear transducer in this research. As the element size is 0.046 cm, the transducer length of 5.56 cm consists of 121 elements.

Figure 11 shows the pressure obtained in the FP, for different transducer lengths in three depths. It is clear that by increasing the length after some values, the pressure of FP reaches to a constant value in each depth. The saturating of pressure happens earlier for small depths. There is no pressure saturation in the absence of the bone layer, so this saturation is related to the bone layer. One of the main reason for this phenomenon, is the critical angle reflection law. Consider the line connecting the last element to the FP in Figure 1. We defined the angle between this line and the line perpendicular to the bone layer as the incident angle (θ_i) as shown in Figure 1. By adding a new element to the end of the transducer, the incident angle is increased. By reaching the angle to the critical angle, the significant portion of the waves are reflected, and they do not have any effect on the pressure of the FP. The critical angle (θ_c) is calculated using Equation (1) which is equal to 29.176 degree.

$$\theta_c = \arcsin\left(\frac{\text{sound speed}_{\text{brain}}}{\text{sound speed}_{\text{bone}}}\right) \quad (1)$$

There is a transducer length, for each focus depth, such that the waves that propagated from the outermost elements will incident with θ_c . So, there is no change in the FP pressure after this length. As an example, for the focus depth of 4.6 cm, this length is obtained 11.64 cm, using θ_c , which is proven in Figure 11. As the depth increases, the critical angle appears for a greater transducer length. In other words, the optimized length is greater for deeper focus point (Figure 10a). Hence, the pressure saturation happens earlier for the lower depth (Figure 11).

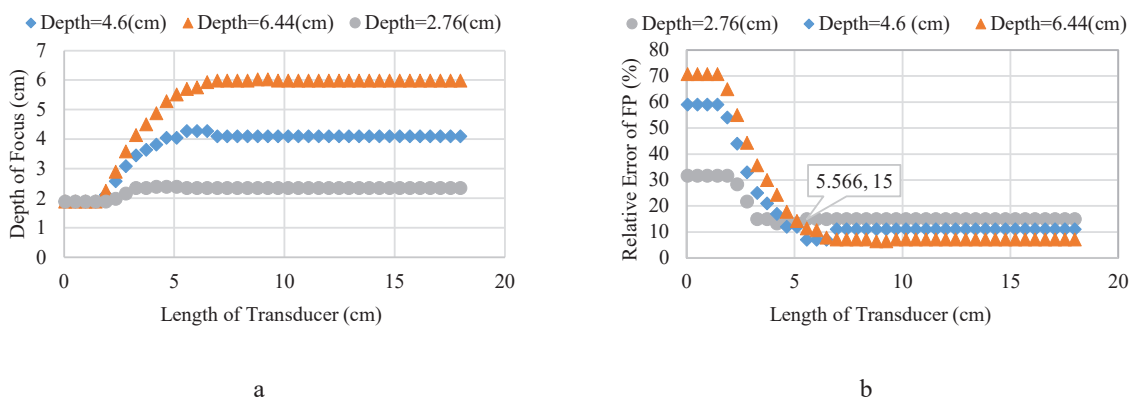


Figure 10. a) The depth of FP and b) The relative error of the focus depth as a function of transducer length for three different desired depths.

Figure 12 shows the targeting error in different depths, for six different element length. It is shown that, by increasing the length of each element, the error rate of the FP position is increased in the most cases. The increasing of grating lobes by

increasing the element length is one of the reason for the reduction in targeting accuracy. By defining the element length more than 0.156 cm ($\lambda/2$) we observe some grating lobes.

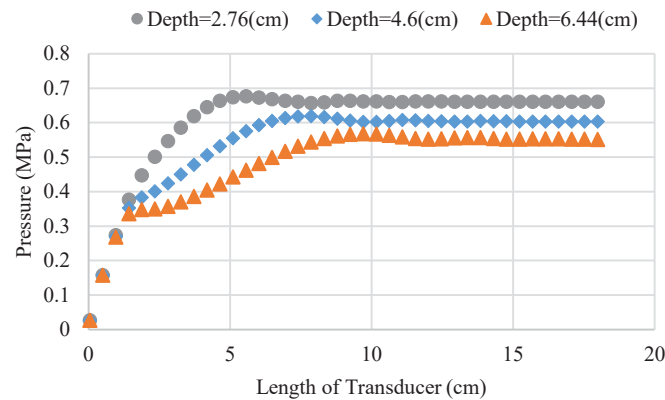


Figure 11. The pressure of the FP as a function of the transducer length for three different desired depths of focus.

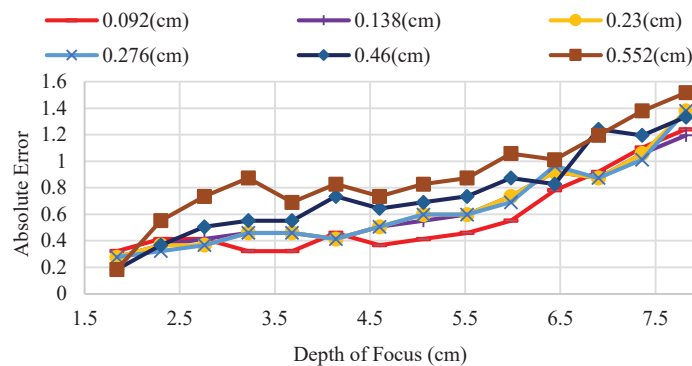


Figure 12. Absolute error of position of FP in different depths for 6 different element sizes.

3.6. The Effect of Depth, Bone Thickness and Input Pressure on Amplitude of Focus Pressure

We tended to determine the amplitude of pressure of transducer elements so that the desired pressure of the focus point can be reached. But according to our investigations, the depth of focus and thickness of bone affects the pressure of the focus point. Hence, we considered these four parameters in our studies and we set up some simulations with different values of these parameters to study the relationship between them.

After getting data from 770 different cases, we plotted our output (the pressure of FP) as a function of focus depth, bone thickness, and input amplitude. The results are shown in Figure 13, Figure 14 and Figure 15, respectively. In these figures, in each step, we have considered the depth, thickness, and amplitude, separately. Then, for different values of other two parameters, we have captured the amplitude of pressure (FP pressure). As indicated in these figures, all these parameters affect the amplitude of pressure. However, it is clear that it is not possible to obtain an independent relation

between one of these parameters and amplitude of pressure. It is easy to understand that there exists a multi-variable function or relation that depends on the depth, thickness and input amplitude. So, we need to consider the effect of all the parameters simultaneously in order to study how the amplitude of pressure in the FP behaves.

To obtain a fitness function estimating the relation of investigated parameters, we used MLP. By this approach, we found a model with 0.99 correlation coefficient and 0.01 mean absolute error (Table 2) that shows it is a powerful model. To prove the efficiency of our model, we repeated the simulation. By using our model, we determined the input amplitude for different desired amplitudes of pressure in the FP. The simulation includes 77 cases (7 thickness and 11 depths) for each input amplitude. After that, we recorded the focus pressure (pressure in the focus point), by the function of desired focus pressure.

We calculated the relative error of output pressure by our desired amplitude pressure using Equation (2).

$$E_r = (|P_d - P_s| * 100)/P_d \quad (2)$$

In this equation, the P_d is the desired pressure, which is expected in the FP. The P_s is the pressure we get from the k-wave as the pressure of FP. Figure 16, illustrates the maximum relative error of the pressure of FP for each desired pressure. For most of the cases, we reach to a pressure nearly equals to our desired pressure, especially for amplitudes of 0.6 to 1.4 MPa that the maximum relative error

is 2.92%. The maximum error (13.7%) belongs to the deepest point and amplitude of 2.2 MPa. However, the average error rate reported is less than 1.8 percent.

As depicted in Figure 16, the maximum error is not similar for different desired pressure values. The relative error of training data is less for the FP pressure and ranged from 0.6 to 1.4 MPa. It means that, at these ranges, the MLP leads us to achieve the desired pressure in the FP with high accuracy. However, for another desired FP that are out of mentioned range, the error is greater. It means that the difference between the desired FP pressure and the FP pressure obtained from MLP is significant. To find the origin of this problem, we looked at the distribution of our training data based on the FP pressure for MLP. To plot the distribution, we divided the data into 9 equal-width bins. For each bin, which has 0.3 width, the number of samples within the range are counted. Figure 17 shows the histogram of the FP pressure distribution. It is clear that the distribution of FP pressures is neither uniform nor normal. The first and the last two bins have 22 and 9 samples, respectively. This is less than 4.1% of all the training data, which is dramatically low; and makes it hard for MLP to be trained over the samples in these ranges. Whereas, the other seven bins have relatively enough samples such that more than 95% of the data are included. Therefore, the NN can be trained more effectively in these ranges and gives us the desired FP with a lower error.

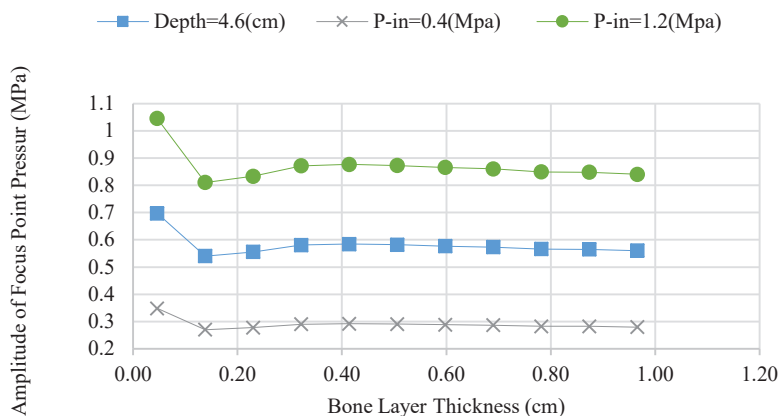


Figure 13. Obtained pressure of FP as a function of the thickness for two different input pressure amplitudes (0.4 and 1.2 MPa when the focus depth is 4.6 cm) and one depth(4.6 cm when the input pressure is 0.8 MPa).

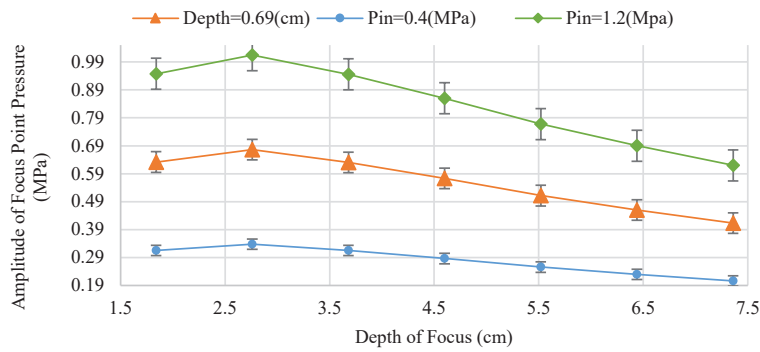


Figure 14. Obtained pressure of FP based on depth of focus for two different input pressure amplitudes (0.4 and 1.2 MPa when the bone thickness is 0.69 cm) and one bone thickness (0.69 cm when the input pressure is 0.8 MPa).

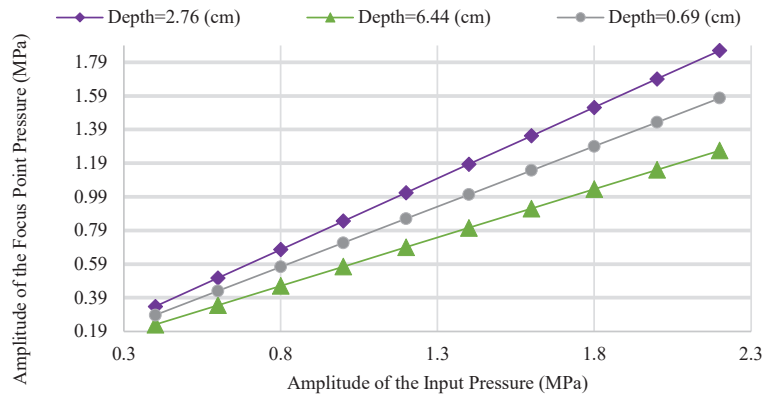


Figure 15. Obtained pressure of FP as a function of the input pressure amplitudes for one thickness (0.69 cm when the focus depth is 4.6 cm) and two different depths (2.76 and 6.44 cm when the bone thickness is 0.69 cm). the relation of input pressure and focus pressure is approximately linear.

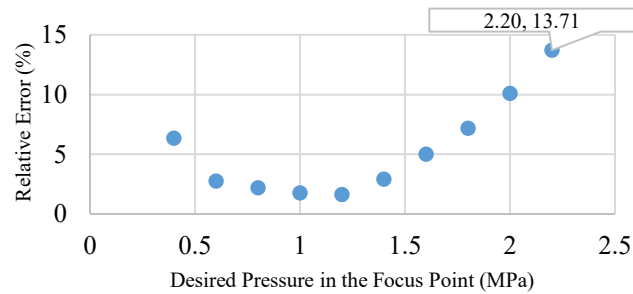


Figure 16. Relative error of pressure of focus point for 10 different values of desired pressure.

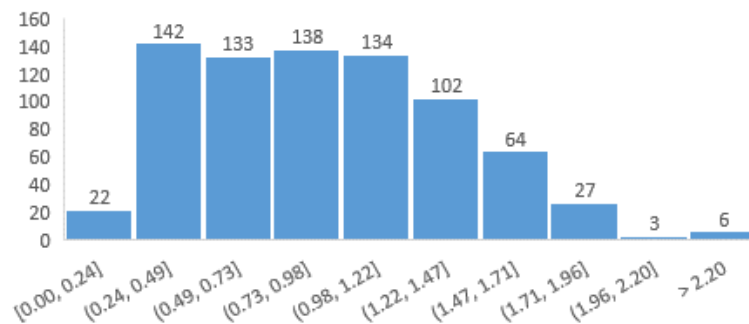


Figure 17. The histogram of distributed FP pressure data for neural network training.

4. Conclusions

Transcranial Focused Ultrasound (tFUS) is a safe method, with high resolution to stimulate the brain tissue. In most of the experiments, the transducers used for stimulation are single-element. However, using a Phased Array Transducer (PATr) enables us to focus on high resolution in the desired position, without moving the transducer by appropriate beam-forming.

This research attempted to simulate the physical condition of the waves propagation in the brain. Since the PATr helps focus on appropriate beam-forming, we used a linear PATr to focus the waves in the simple simulated environment of the head. We proposed considering all tissues with their heterogeneities in time delays calculation before the tFUS. This improves the targeting accuracy. After using this method, the FP displacement for different thickness of the bone layer was reduced. The results of optimization showed that the maximum relative error of FP is about 16.25 percent, such that a significant improvement of about 32 units is obtained.

In the next step, we investigated the length of the transducer on the position of the FP. We have obtained the minimum possible length of the transducer in which we can focus on different positions with an acceptable error rate of the FP displacement. This value was 5.56 cm. Also, we investigated how the element length of PATr affects the FP. According to our results, by increasing the length of each element, the error rate of the FP position is generally increased.

As the last step, we used the MLP algorithm to present a model that helped us find the appropriate amplitude of pressure of transducer elements. This led to reach the desired pressure in FP.

Since manufacturing of PATrs is easier and cheaper than before [21], we can design a PATr for a specific application. Therefore, we need to investigate the parameters of designing PATr which affect the tFUS procedures. Then, we can manufacture our desired PATr according to these parameters. Based on our results, we presented some characteristics of a linear transducer that can be used in the context of brain stimulation, for treatment and brain mapping purposes. These parameters include the length of the transducer,

element length, the amplitude of input signal, and the appropriate beam-forming which is tissue-sensitive in order to focus more precisely.

References

- 1- J.-P. Lefaucheur, "Principles of therapeutic use of transcranial and epidural cortical stimulation," *Clinical Neurophysiology*, vol. 119, no. 10, pp. 2179-2184, 2008.
- 2- H. A. Sackeim and M. S. George, "Brain stimulation—basic, translational, and clinical research in neuromodulation: Why a new journal?," *Brain Stimulation: Basic, Translational, and Clinical Research in Neuromodulation*, vol. 1, no. 1, pp. 4-6, 2008.
- 3- T. Wagner, A. Valero-Cabre, and A. Pascual-Leone, "Noninvasive human brain stimulation," *Annu. Rev. Biomed. Eng.*, vol. 9, pp. 527-565, 2007.
- 4- P. Limousin *et al.*, "Electrical stimulation of the subthalamic nucleus in advanced Parkinson's disease," *New England Journal of Medicine*, vol. 339, no. 16, pp. 1105-1111, 1998.
- 5- R. Pashaie *et al.*, "Optogenetic brain interfaces," *IEEE reviews in biomedical engineering*, vol. 7, pp. 3-30, 2014.
- 6- R. L. King, Julian R. Brown, William T. Newsome, and Kim Butts Pauly, "Effective parameters for ultrasound-induced in vivo neurostimulation," *Ultrasound in medicine and biology*, vol. 39, pp. 312-331 2013.
- 7- I. Moreno-Duarte, L. R. Morse, M. Alam, M. Bikson, R. Zafonte, and F. Fregni, "Targeted therapies using electrical and magnetic neural stimulation for the treatment of chronic pain in spinal cord injury," *Neuroimage*, vol. 85, pp. 1003-1013, 2014.
- 8- W. J. Tyler, Y. Tufail, M. Finsterwald, M. L. Tauchmann, E. J. Olson, and C. Majestic, "Remote excitation of neuronal circuits using low-intensity, low-frequency ultrasound," *PloS one*, vol. 3, no. 10, p. e3511, 2008.
- 9- Y. Tufail, Alexei Matyushov, Nathan Baldwin, Monica L. Tauchmann, Joseph Georges, Anna Yoshihiro, Stephen I. Helms Tillery, and William J. Tyler, "Transcranial pulsed ultrasound stimulates intact brain circuits," *Neuron* vol. 66, no. 5, pp. 681-694 2010.
- 10- S.-S. Yoo, Alexander Bystritsky, Jong-Hwan Lee, Yongzhi Zhang, Krisztina Fischer, Byoung-Kyong Min, Nathan J. McDannold, Alvaro Pascual-Leone, and Ferenc A. Jolesz, "Focused ultrasound modulates

- region-specific brain activity," *Neuroimage*, vol. 56, no. 3, pp. 1267-1275, 2011.
- 11- A. P. Mulgaonkar, Singh, R. S., Babakhanian, M., Culjat, M. O., Grundfest, W. S., Gorgulho, A., ... & Melega, W. P., "A prototype stimulator system for noninvasive Low Intensity Focused Ultrasound delivery," in *MMVR* 2012, pp. 297-303.
- 12- W. Lee, Kim, H., Jung, Y., Song, I. U., Chung, Y. A., & Yoo, S. S., "Image-guided transcranial focused ultrasound stimulates human primary somatosensory cortex," *Scientific reports*, vol. 5, 2015.
- 13- W. Legon, Tomokazu F. Sato, Alexander Opitz, Jerel Mueller, Aaron Barbour, Amanda Williams, and William J. Tyler, "Transcranial focused ultrasound modulates the activity of primary somatosensory cortex in humans," *Nature neuroscience*, vol. 17, no. 2, pp. 322-329 2014.
- 14- J. K. Mueller, L. Ai, P. Bansal, and W. Legon, "Computational exploration of wave propagation and heating from transcranial focused ultrasound for neuromodulation," *Journal of neural engineering*, vol. 13, no. 5, p. 056002, 2016.
- 15- J. Kim, and Sungon Lee, "Development of a Wearable Robotic Positioning System for Noninvasive Transcranial Focused Ultrasound Stimulation," *IEEE/ASME Transactions on Mechatronics* vol. 21, no. 5, pp. 2284-2293, 2016.
- 16- W. Lee, et al, "Transcranial focused ultrasound stimulation of human primary visual cortex," *Scientific Reports* 2016.
- 17- K. K. Shung, *Diagnostic ultrasound Imaging and blood flow measurements*. CRC press, 2015.
- 18- M. Tanter, J.-L. Thomas, and M. Fink, "Focusing and steering through absorbing and aberrating layers: Application to ultrasonic propagation through the skull," *The Journal of the Acoustical Society of America*, vol. 103, no. 5, pp. 2403-2410, 1998.
- 19- K. Hynynen, Gregory T. Clement, Nathan McDannold, Natalia Vykhodtseva, Randy King, P. Jason White, Shuki Vitek, and Ferenc A. Jolesz, "500-element ultrasound phased array system for noninvasive focal surgery of the brain: A preliminary rabbit study with ex vivo human skulls," *Magnetic resonance in medicine* vol. 52, no. 1, pp. 100-107 2004.
- 20- H.-L. Liu, Heng-Wen Chen, Zhen-Hao Kuo, and Wen-Cheng Huang, "Design and experimental evaluations of a low-frequency hemispherical ultrasound phased-array system for transcranial blood-brain barrier disruption," *IEEE transactions on biomedical engineering*, vol. 55, no. 10, pp. 2407-2416 2008.
- 21- W. Law, T. Sato, and W. J. Tyler, "Thin and wearable ultrasound phased array devices," ed: Google Patents, 2015.
- 22- T. D. Mast, L. P. Souriau, D.-L. Liu, M. Tabei, A. I. Nachman, and R. C. Waag, "A k-space method for large-scale models of wave propagation in tissue," *IEEE transactions on ultrasonics, ferroelectrics, and frequency control*, vol. 48, no. 2, pp. 341-354, 2001.
- 23- B. E. Treeby, J. Jaros, A. P. Rendell, and B. Cox, "Modeling nonlinear ultrasound propagation in heterogeneous media with power law absorption using ak-space pseudospectral method," *The Journal of the Acoustical Society of America*, vol. 131, no. 6, pp. 4324-4336, 2012.
- 24- J. L. Robertson, B. T. Cox, and B. E. Treeby, "Quantifying numerical errors in the simulation of transcranial ultrasound using pseudospectral methods," in *Ultrasonics Symposium (IUS), 2014 IEEE International*, 2014, pp. 2000-2003: IEEE.
- 25- X. Yin, and Kullervo Hynynen, "A numerical study of transcranial focused ultrasound beam propagation at low frequency," *Physics in medicine and biology* vol. 50, no. 8, p. 1821, 2005.
- 26- A. Moreira-Gonzalez, F. E. Papay, and J. E. Zins, "Calvarial thickness and its relation to cranial bone harvest," *Plastic and reconstructive surgery*, vol. 117, no. 6, pp. 1964-1971, 2006.
- 27- C. M. Bishop, *Pattern recognition and machine learning*. springer, 2006.
- 28- R. Kohavi, "A study of cross-validation and bootstrap for accuracy estimation and model selection," in *Ijcai*, 1995, vol. 14, no. 2, pp. 1137-1145: Stanford, CA.
- 29- K. Hornik, M. Stinchcombe, and H. White, "Multilayer feedforward networks are universal approximators," *Neural networks*, vol. 2, no. 5, pp. 359-366, 1989.
- 30- E. Frank and R. R. Bouckaert, "Conditional density estimation with class probability estimators," in *Asian Conference on Machine Learning*, 2009, pp. 65-81: Springer.
- 31- R. J. Quinlan, "Learning with Continuous Classes " in *5th Australian Joint Conference on Artificial Intelligence*, 1992.
- 32- S. R.J, *Pattern recognition*. John Wiley & Sons, Inc, 1992.

33- A. R. Barron, "Approximation and estimation bounds for artificial neural networks," *Machine Learning*, vol. 14, no. 1, pp. 115-133, 1994.

34- J. Mueller, Wynn Legon, Alexander Opitz, Tomokazu F. Sato, and William J. Tyler, "Transcranial focused ultrasound modulates intrinsic and evoked EEG dynamics," *Brain stimulation*, vol. 7, no. 6, pp. 900-908 2014.